Atomistic Origin of Brittle Failure of Boron Carbide from Large-Scale Reactive Dynamics Simulations: Suggestions toward Improved Ductility

Qi An and William A. Goddard III*
Materials and Process Simulation Center, California Institute of Technology, Pasadena, California 91125, United States

(Received 19 May 2015; revised manuscript received 1 July 2015; published 31 August 2015)

Ceramics are strong, but their low fracture toughness prevents extended engineering applications. In particular, boron carbide (B_4C), the third hardest material in nature, has not been incorporated into many commercial applications because it exhibits anomalous failure when subjected to hypervelocity impact. To determine the atomistic origin of this brittle failure, we performed large-scale (~200 000 atoms/cell) reactive-molecular-dynamics simulations of shear deformations of B_4C, using the quantum-mechanics-derived reactive force field simulation. We examined the $(0001)/\langle 10\bar{1}0\rangle$ slip system related to deformation twinning and the $(01\bar{1}\,\bar{1})/\langle\bar{1}101\rangle$ slip system related to amorphous band formation. We find that brittle failure in B_4C arises from formation of higher density amorphous bands due to fracture of the icosahedra, a unique feature of these boron based materials. This leads to negative pressure and cavitation resulting in crack opening. Thus, to design ductile materials based on B_4C we propose alloying aimed at promoting shear relaxation through intericosahedral slip that avoids icosahedral fracture.

DOI: 10.1103/PhysRevLett.115.105501 PACS numbers: 62.20.mj, 62.20.mm, 81.05.Je

Engineering ceramics, such as boron carbide, silicon carbide, and alumina exhibit higher strength than metals, making them candidate materials for such extreme conditions applications as body armor [1,2]. A key parameter for assessing the potential of ceramic materials for high stress applications is the Hugoniot elastic limit (HEL) [3], the yield point for uniaxial elastic compression. With an HEL of 18–20 GPa boron carbide (B_4C) has the best resistance to hypervelocity impact among common ceramics. Thus, B_4C with its combination of other important properties such as high thermal stability, high hardness, and low density [3–13], was considered to be an ideal armor material. However, experimental dynamics experiments on B_4C show abnormal low fracture toughness above a critical speed of ~900 m/s [9], which would not be expected from such a high HEL. The origin of this poor behavior in boron carbide remains a mystery although it was discovered 80 years ago.

Two hypotheses to explain the brittle failure behaviors in B_4C at hypervelocity impact and high pressure are (a) it results from the low density or (b) it results from a phase transition. No convincing evidence has been advanced to support these hypotheses [14]. A major advance is the recent observation of local amorphization bands (1–3 nm wide and 100–200 nm long) that form during hypervelocity impact and nanoindentation experiments [9–13]. Thus, it has been postulated that the amorphous bands are responsible for the brittle failure [9]. Several theoretical studies have applied density functional theory (DFT) to determine the structural changes responsible for amorphous band formation [14–16], but none could directly observe amorphous band formation (because DFT was limited to hundreds of atoms). Thus, it remains unclear how amorphous band formation is related to the mechanism of brittle failure.

Herein, we investigate why thin 1–3 nm amorphous bands change the mechanical properties so dramatically, obtaining an alternative explanation for brittle failure of B_4C. In order to determine the origin of the low fracture toughness for B_4C, we carried out reactive molecular dynamics (RMD) simulations on finite shear deformations of B_4C at room temperature using periodic cells with ~200 000 atoms. We continued to shear the system until failure for two different slip systems (i) $(0001)/\langle 10\bar{1}0\rangle$ chosen because it is related to deformation twinning [17], and (ii) $(01\bar{1}\,\bar{1})/\langle\bar{1}101\rangle$ because it is related to amorphous band formation [13,16].

We found that the deformation mechanism along the $(0001)/\langle 10\bar{1}0\rangle$ slip system involves a sequence of discrete twinning formation steps, followed eventually by amorphous band formation, cavitation, and crack opening. In contrast, no twin formation is observed for the $(01\bar{1}\,\bar{1})/\langle\bar{1}101\rangle$ slip system prior to amorphous band formation, after which we observe cavitation, and eventually crack opening.

This analysis of the failure process shows that the origin of the brittle failure fracture for B_4C is the formation of *higher density* amorphous bands that lead to negative pressures, cavitation, and eventually crack opening. The high density of the amorphous structures is further confirmed by the *ab initio* molecular dynamics (AIMD) simulations.

The B_4C structure shown in Fig. 1(a) is based on α boron, a rhombohedral structure [18]. There are several ways to distribute the C atoms but the most stable one is $(B_{11}C_p)(CBC)$ [16], which indicates one $(B_{11}C)$

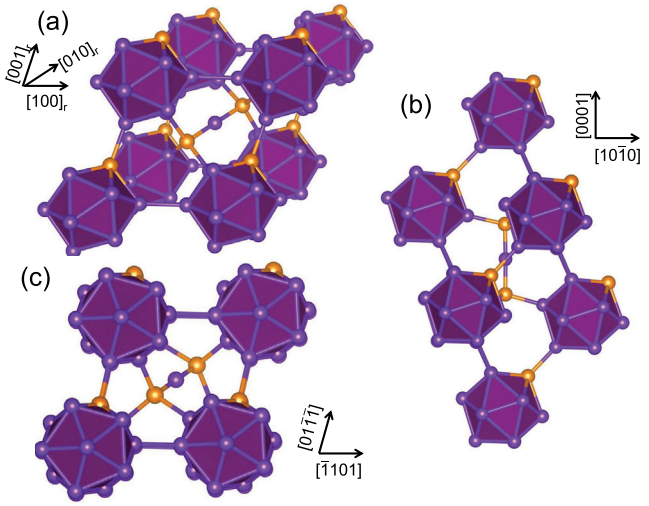

FIG. 1 (color online). (a) Rhombohedral structure of B_4C, showing one unit cell. B atoms are purple and C atoms are bronze. (b) $(0001)/\langle 10\bar{1}0\rangle$ slip system that leads initially to twin formation and eventually amorphous band formation along the (0001) plane. (c) $(01\bar{1}\,\bar{1})/\langle\bar{1}101\rangle$ slip system that leads to amorphous band formation along the $(01\bar{1}\,\bar{1})$ plane.

icosahedron and one (CBC) chain per unit cell. Each icosahedron can be considered to be in a closest packed plane of icosahedra stacked *ABCABC* (cubic close packing) along the rhombohedral axis. Each icosahedron is bonded to 6 different CBC chains through equatorial (e) sites while also forming 6 direct bonds to 6 icosahedra through polar (p) sites.

In order to retain nearly the accuracy of quantum mechanics (QM) calculations while enabling practical studies of systems sufficiently large to allow formation of the ~2 nm wide twin bands and amorphous bands it is necessary to use periodic cells larger than 20 nm, leading to ~200 000 atoms. Consequently, we used the reactive force field simulation (ReaxFF) [19] trained to reproduce the structures, energy, and reaction barriers from QM. ReaxFF has enabled the simulation of complex reactive systems, for example, shock decompositions involving 3.7×10^6 atoms per periodic cell to identify the origin of hot spots formation in plastic-bonded explosives [20]. To determine the parameters for ReaxFF, we fitted (i) the QM derived interactions of two icosahedra ($B_{10}C_2H_{12}$), (ii) the equations of state (EOS) of various boron phases (α-B_{12}, γ-B_{28}, T-B_{50}), (iii) the EOS of three stoichiometries of B_4C ($(B_{11}C_p)$(CBC), $(B_{11}C_e)$(CBC), and (B_{12})(CCC)), (iv) the heat of formation of various boron and B_4C phases, and (v) the shear deformation of $(B_{11}C_p)$(CBC) shearing along $(01\bar{1}\,\bar{1})/\langle\bar{1}101\rangle$ that leads to amorphous structure. We could not fit directly to twin formation simulations from QM, because the QM unit cells were too small to accommodate transformation to a finite twin. Thus, we expect that ReaxFF leads to a reasonable description of shear deformations in B_4C. We also developed a second ReaxFF force field, denoted ReaxF2, in which the shear stress behavior from QM was included in the training set. This led to an improved description of elastic constants but led to the same deformation mechanism. The parameters for ReaxF2 and comparison of the twin formation and amorphous failure detail are in the Supplemental Material [21].

Figure 1(b) shows the unit cell for shearing along the $(0001)/\langle 10\bar{1}0\rangle$ slip system expected to be favorable for formation of twins along the (0001) plane, where the CBC chains are perpendicular to the slip direction. The simulation model has cell lengths of $a = 29.4$, $b = 2.2$, and $c = 24.0$ nm, leading to 216 000 atoms (14 400 formula units). The periodic boundary conditions are applied along all three directions. Here we changed the unit cell angle without changing box volume during shear simulation. This leads to negative pressure (tensile condition). We use a negative sign in the shear stress to be consistent with negative pressure. The simulation details are in the Supplemental Material [21].

Figure 2(a) displays the shear-stress–strain relations for shear deformation along the $(0001)/\langle 10\bar{1}0\rangle$ slip system, along with the total pressure (P). The deformation mechanism involves the following steps. (i) The shear stress τ and P become more negative continuously during the elastic region, reaching $\tau = -26.1$ and $P = -10.0$ GPa at 0.269 strain. (ii) Twin bands initiate [Fig. 2(b)] from 0.269 to

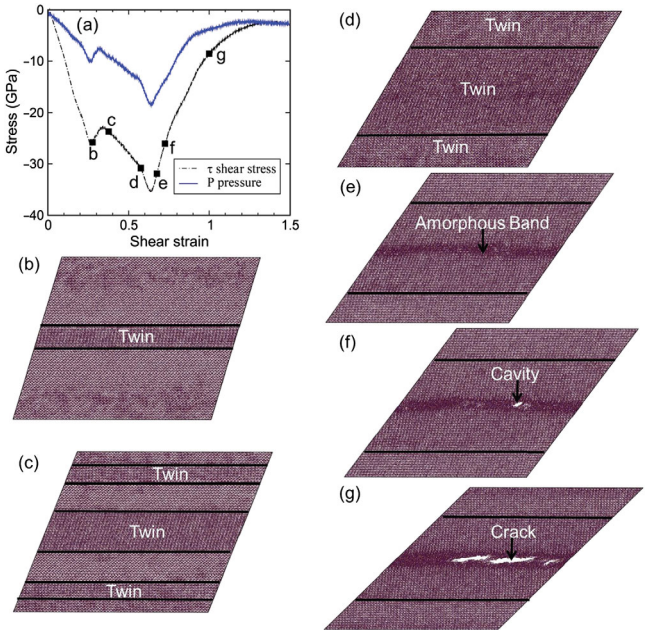

FIG. 2 (color online). Stress-strain relations and snapshots for shear along slip system $(0001)/\langle 10\bar{1}0\rangle$, showing the successive processes of twinning, amorphous band formation, and cavitation. The twin boundaries are represented by the solid black line. (a) Stress-strain relations. (b) Twin formation at 0.275 strain. (c) Twin growth and new twins form at 0.375 strain. (d) Two twins grow to the whole cell at 0.575 strain. (e) Amorphous band formation within the twinned region at 0.675 strain. (f) Cavitation within the amorphous band at 0.725 strain. (g) Full crack formation by 1.00 strain.

0.328 strain, over which range τ decreases slightly to −23.0 and P decreases to −7.8 GPa. (iii) As the twin region increases [Fig. 2(c)] up to a total width of ∼6 nm, two additional twin regions form at a shear strain of 0.375, at which point τ increases to −23.7 and P increases to −9.1 GPa. The computed shear stress within the twin grains is 34.1 GPa, which is larger than the 21.0 GPa for the region outside the twin grains. This indicates a rotation of the grains of the twin region relative to the applied shear stress. (iv) Two twin regions grow continuously to the whole cell to form a new twin boundary [Fig. 2(d)] at a shear strain of 0.575, where τ and P increase to −30.8 and −14.1 GPa, respectively. (v) At this point, an amorphous band forms along the whole simulation cell as shown in Fig. 2(e) for 0.675 strain. This amorphous band forms within the original twinned region, where the icosahedra are distorted. Amorphous band formation dramatically relieves both the shear stress and the pressure. (vi) a cavity forms [Fig. 2(f)] within the amorphous band at 0.725 strain to continue the stress relaxation. (vii) Finally, a crack opens [Fig. 2(g)] that further relaxes the stresses to $\tau = -8.6$ and $P = -3.7$ GPa at a strain of 1.0.

In order to analyze the structural changes during shearing, we computed the radial distribution function (RDF) within a 2 nm wide 1D bin along the shear direction that includes the twin and the amorphous structures at various strains. As shown in Fig. 3(a), a number of peaks appear in the RDF spectra of the intact structure, representing the complex atomic configurations of B_4C. As the shear increases to 0.375 strain at which twinned structures form, most peaks remain in the RDF, although it is smoother than for the perfect crystal. This indicates that the twinned structure remains ordered. However, as the shear is increased to 0.675 strain to initiate the amorphous band, the RDF exhibits a typical amorphous character with only one obvious peak, indicating fractured icosahedra.

Figure 1(c) shows the unit cell for shearing along $(01\bar{1}\,\bar{1})/\langle\bar{1}101\rangle$, which is expected to favor amorphous band formation [13,16]. The simulation model has cell lengths of $a = 26.2$, b = 2.6, and $c = 24.5$ nm, leading to 187 500 atoms (12 500 formula units). Here the shear stress becomes more negative continuously to −45.0 GPa at a strain of 0.375, as shown in Fig. S1 of the Supplemental Material [21]. Then, the stress is relaxed by structural distortions that form an amorphous band. Figure 4 shows the structural changes for this slip system. Figure 4(a) shows the structure at 0.2 strain where no defects have formed within the elastic deformation region. Figure 4(b) displays the structural distortion at 0.4 strain where the stress starts to relax. Then Fig. 4(c) shows that an amorphous band forms at 0.5 strain, which is accompanied by nearby stacking faults. Finally, cavitation initiates [Fig. 4(d)] within the amorphous band at 1.25 strain. This cavitation leads to crack opening at 1.75 strain [Fig. 4(e)]. The maximum shear stress for $(01\bar{1}\,\bar{1})/\langle\bar{1}101\rangle$ slip is 45.0 GPa, which is higher than the value of 35.3 GPa for $(0001)/\langle10\bar{1}0\rangle$ slip, indicating that amorphous bands form more easily within the twinned structure for which the icosahedra have already distorted.

The maximum shear stress of 45.0 GPa for this $(01\bar{1}\,\bar{1})/\langle\bar{1}101\rangle$ simulation with 187 500 atoms is much higher than the ideal shear stress of 37.2 GPa from our previous DFT study [16] because these ReaxFF studies keep the cell volume fixed. ReaxFF studies for $(01\bar{1}\,\bar{1})/\langle\bar{1}101\rangle$ shear, but allowing relaxation of the normal stresses decreases the maximum shear stress from 45.0 to 34.4 GPa, similar to the 37.2 GPa from our QM studies (Fig. S1 of Supplemental Material [21]). However, ReaxFF simulations for $(0001)/\langle10\bar{1}0\rangle$ shear, and also allowing relaxation of the normal stresses increase the maximum shear stress from 35.3 to 43.2 GPa, as shown in Fig. S1 of the Supplemental Material [21]. Thus stress relaxation increases the stress barrier for twin formation by opposing grain rotation. The higher twin formation barrier increases the shear stress barrier for forming the amorphous band. Thus, the slip system $(01\bar{1}\,\bar{1})/\langle\bar{1}101\rangle$ is easier to activate in normal stress relaxation conditions, consistent with the experimental observations [13] and QM study [16].

To extract the origin of cavitation and brittle failure during shear deformation, we partitioned the simulation cell into 10 bins along the c directions and averaged the density within each bin, as shown in Fig. 3(b) for slip along $(01\bar{1}\,\bar{1})/\langle\bar{1}101\rangle$. Figure 3(d) shows that the amorphous band formed without prior twinning leads to a density of 2.70 g/cm^3, compared to 2.55 g/cm^3 for the bulk. In contrast, the amorphous band formed within the twinned bands for $(0001)/\langle10\bar{1}0\rangle$ leads to a maximum density of 2.64 g/cm^3 [Fig. 3(c)] indicating that the deformations involved in twin formation lead to a smaller increase in density for the amorphous band. In both systems the higher density within the amorphous band provides the free volume for cavitation under negative pressures. Thus, the origin of brittle failure in boron carbide is the increase in density due to icosahedral fracture that provides the free volume and negative pressure needed for amorphous band formation.

The detailed evolution of the amorphous band is as follows. At the high strain rate deformation, three layers of local icosahedra with ∼2 nm width start to collapse. This increases the local shear strain dramatically, causing the collapse region to propagate quickly throughout the whole simulation cell (∼29 nm) within 0.5 ps to form an amorphous band traversing the whole cell. This effectively changes the boundary conditions of the surrounding crystalline region, where the unbroken icosahedra are bonded to the broken cages in the boundary, accommodating the vertical relaxation to the amorphous band. As the amorphous band forms, it starts to contract because of its higher density compared to the surrounding crystalline phase, leading to the cavity formation.

To verify our conclusions about the density changes from these ReaxFF simulations on systems with

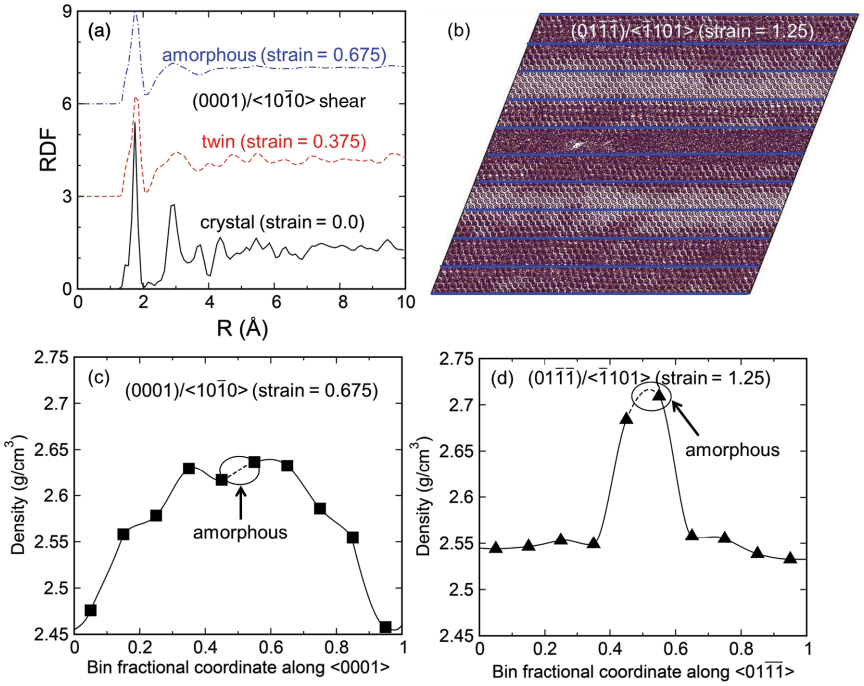

FIG. 3 (color online). The structural and density analysis under shear along slip systems of $(0001)/\langle 10\bar{1}0\rangle$ and $(01\bar{1}\,\bar{1})/\langle\bar{1}101\rangle$. (a) The RDF of the 2 nm band that includes the twinned or amorphous band region for the shear along $(0001)/\langle 10\bar{1}0\rangle$. (b) Snapshot for 1.25 shear strain along $(01\bar{1}\,\bar{1})/\langle\bar{1}101\rangle$, with the 1D bins shown by solid blue lines. (c) The 1D density profile along the $\langle 0001\rangle$ axis for 0.675 shear strain along $(0001)/\langle 10\bar{1}0\rangle$ at which the amorphous band initiates. (d) The 1D density profile along the $\langle 01\bar{1}\,\bar{1}\rangle$ axis for the 1.25 shear strain along $(01\bar{1}\,\bar{1})/\langle\bar{1}101\rangle$, at which the amorphous band initiates, corresponding to the snapshot in (b). The amorphous regions in (c) and (d) are represented by the black circle.

~200 000 atoms/cell, we carried out AIMD simulations using forces from DFT at the PBE level on systems with 120 atoms/cell to extract the equations of state (EOS) for both crystalline phases and amorphous phases. The simulation details are in the Supplemental Material [21]. We refer to the amorphous structure obtained by shear deformation along the $(01\bar{1}\,\bar{1})/\langle\bar{1}101\rangle$ slip system [16] as the *sheared* amorphous phase. We heated this amorphous structure to 3000 K to melt it and then quenched it back to form the *annealed* amorphous phase. We applied hydrostatic compression to the crystalline structure and to the two amorphous phases, as shown in Fig. S2 of Supplemental Material [21]. We find that with 35 GPa compression, the sheared amorphous phase has a density of 2.908 g/cm^3, just slightly below the density of 2.951 g/cm^3 for the annealed amorphous phas—both of which are substantially higher (by ~2.3% and ~3.9%) than the 2.841 g/cm^3 for the crystalline phase at this pressure. The density differences increase to ~4% and 5% for two amorphous phases under a pressure of 50 GPa and increase continuously at higher pressures. This indicates that higher pressure increasingly favors amorphous band formation, leading to cavitation and eventually brittle failure.

These studies indicate that to improve the ductility of boron carbide, we need to allow deformation to accommodate stress relaxation while avoiding fracturing the icosahedra that leads to the increased density of the amorphous band. We find that an amorphous band forms more easily at twinned regions where predistorted icosahedra exist. This suggests that the amorphous bands might form more easily within other defect structures, such as stacking faults (SF) and grain boundaries (GBs). Thus, the

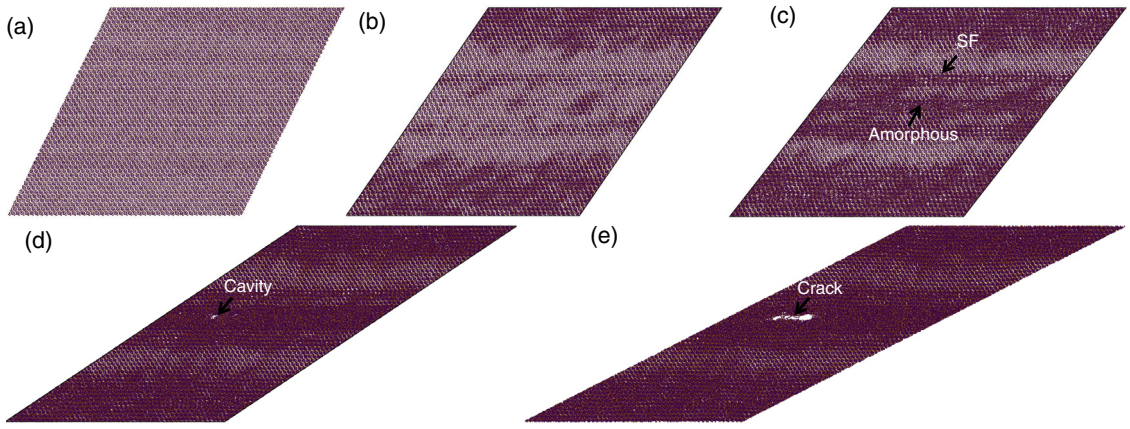

FIG. 4 (color online). Snapshots for shear along the $(01\bar{1}\,\bar{1})/\langle\bar{1}101\rangle$ slip system at various strains. (a) $s = 0.2$, (b) $s = 0.4$, (c) $s = 0.5$, (d) $s = 1.25$, and (e) $s = 1.75$.

design strategy to achieve ductile B_4C should avoid stress concentrations due to such defect regions under high strains. Consequently, we need to find synthesis conditions that produce GBs that can shear without stress concentrations. Our previous QM studies on $2 \times 2 \times 2$ supercells showed that replacing the CBC chain with Si-Si two-atom chains or with O single-atom chains permits very large strain in single crystals without breaking the icosahedra [29,30]. In these cases the Si_2 or O chains form bonds to 3 icosahedra, which during shear allow some bonds to move from one icosahedron to another while other bonds keep the structures intact. That is, the chains walk along the icosahedra (*log rolling*) as the shear planes continually displace neighboring icosahedra to become farther away. This suggests that alloying can be directed toward increasing the stability within the icosahedra while incorporating chains that can bond between multiple icosahedra to log roll as the shear proceeds.

These observations lead us to suggest that an important design consideration for stabilizing the icosahedra would be to modify the composition to guarantee that 26 electrons providing tangential bonding within each icosahedron (Wade's rule) remain independent of the shearing. For $(B_{11}C_p)(CBC)$ under shear deformation of the chain leads to bonding of the central B to additional icosahedral atoms [16], decreasing the effective electron count from 26, weakening the icosahedra. To avoid this we suggest that the chains have only one or two atoms and chosen so that they need not donate an electron to the icosahedra to satisfy Wade's rule. For example $(B_{10}C_2)(Si_2)$ would have neutral chains and 26 e sites for tangential bonding within the icosahedra. A strategy for synthesizing $(B_{10}C_2)(Si_2)$ is discussed in the Supplemental Material [21].

In summary, we carried out large-scale ($\sim$200 000 atoms/cell) ReaxFF RMD simulations and small scale (120 atoms/cell) AIMD simulations to determine the failure mechanism of B_4C to large shear, starting with perfect crystals. We found that shearing B_4C along $(0001)/\langle 10\bar{1}0\rangle$ leads sequentially to twin formation, amorphous band formation, cavitation, and crack formation, while no twin formation is observed along $(01\bar{1}\,\bar{1})/\langle\bar{1}101\rangle$. The origin of the brittle failure for B_4C is formation of high density amorphous bands from fractured icosahedra that favors negative pressure and cavitation. Our new deformation mechanism explains the abnormal brittle failure of B_4C, providing clues for designing ductile hard materials based on B_4C.

This work was supported by the Defense Advanced Research Projects Agency (W31P4Q-13-1-0010, program manager, Judah Goldwasser) and the National Science Foundation (DMR-1436985). The ReaxFF reactive force field simulation used here was developed with support provided by the Army Research Laboratory under Cooperative Agreement No. W911NF-12-2-0022 (MEDE).

*Corresponding author.
wag@wag.caltech.edu

[1] W. H. Gust and E. B. Royce, J. Appl. Phys. **42**, 276 (1971).
[2] D. E. Munson and R. J. Lawrence, J. Appl. Phys. **50**, 6272 (1979).
[3] N. K. Bourne, Proc. R. Soc. A **458**, 1999 (2002).
[4] A. O. Sezer and J. I. Brand, Mater. Sci. Eng. B **79**, 191 (2001).
[5] F. Thevenot, J. Eur. Ceram. Soc. **6**, 205 (1990).
[6] V. Domnich, S. Reynaud, R. A. Haber, and M. Chhowalla, J. Am. Ceram. Soc. **94**, 3605 (2011).
[7] J. L. Hoard and R. E. Hughes, *The Chemistry of Boron and Its Compounds* (Wiley, New York, 1967).
[8] A. K. Suri, C. Subramanian, J. K. Sonber, and T. Murthy, Int. Mater. Rev. **55**, 4 (2010).
[9] M. W. Chen, J. W. McCauley, and K. J. Hemker, Science **299**, 1563 (2003).
[10] T. J. Vogler, W. D. Reinhart, and L. C. Chhabildas, J. Appl. Phys. **95**, 4173 (2004).
[11] V. Domnich, Y. Gogotsi, M. Trenary, and T. Tanaka, Appl. Phys. Lett. **81**, 3783 (2002).
[12] X. Q. Yan, W. J. Li, T. Goto, and M. W. Chen, Appl. Phys. Lett. **88**, 131905 (2006).
[13] K. M. Reddy, P. Liu, A. Hirata, T. Fujita, and M. W. Chen, Nat. Commun. **4**, 2483 (2013).
[14] G. Fanchini, J. W. McCauley, and M. Chhowalla, Phys. Rev. Lett. **97**, 035502 (2006).
[15] X. Q. Yan, Z. Tang, L. Zhang, J. J. Guo, C. Q. Jin, Y. Zhang, T. Goto, J. W. McCauley, and M. W. Chen, Phys. Rev. Lett. **102**, 075505 (2009).
[16] Q. An, W. A. Goddard III, and T. Cheng, Phys. Rev. Lett. **113**, 095501 (2014).
[17] Y. Li, Y. H. Zhao, W. Liu, Z. H. Zhang, R. G. Vogt, E. J. Lavernia, and J. M. Schoenung, Philos. Mag. **90**, 783 (2010).
[18] V. I. Matkovich, J. Am. Chem. Soc. **83**, 1804 (1961).
[19] A. C. T. van Duin, S. Dasgupta, F. Lorant, and W. A. Goddard III, J. Phys. Chem. A **105**, 9396 (2001).
[20] Q. An, S. V. Zybin, W. A. Goddard III, A. Jaramillo-Botero, M. Blanco, and S. N. Luo, Phys. Rev. B **84**, 220101 (2011).
[21] See Supplemental Material at http://link.aps.org/supplemental/10.1103/PhysRevLett.115.105501, which includes Refs. [22–28], for (i) ReaxFF parameters, (ii) simulation details, (iii) nanocluster strategy for synthesizing $(B_{10}C_2)(Si_2)$, (iv) elastic properties from ReaxFF and its effects on the deformation mechanism, (v) Table S1, and (vi) Figs. S1 to S3.
[22] S. Plimpton, J. Comput. Phys. **117**, 1 (1995).
[23] G. Kresse and J. Hafner, Phys. Rev. B **47**, 558 (1993).
[24] G. Kresse and J. Furthmuller, Comput. Mater. Sci. **6**, 15 (1996).
[25] G. Kresse and J. Furthmüller, Phys. Rev. B **54**, 11169 (1996).
[26] G. Kresse and D. Joubert, Phys. Rev. B **59**, 1758 (1999).
[27] Y. Le Page and P. Saxe, Phys. Rev. B **65**, 104104 (2002).
[28] K. J. Mcclellan, F. Chu, J. M. Roper, and I. Shindo, J. Mater. Sci. **36**, 3403 (2001).
[29] Q. An and W. A. Goddard III, J. Phys. Chem. Lett. **5**, 4169 (2014).
[30] Q. An and W. A. Goddard III, Chem. Mater. **27**, 2855 (2015).